Proc. Natl. Acad. Sci. USA
Vol. 92, pp. 6229–6233, July 1995
Cell Biology

Cotranslational folding and calnexin binding during glycoprotein synthesis

WEI CHEN, JONNE HELENIUS, INEKE BRAAKMAN*, AND ARI HELENIUS

Department of Cell Biology, Yale School of Medicine, 333 Cedar Street, New Haven, CT 06510-8002

Communicated by Vincent T. Marchesi, Yale University, New Haven, CT, March 13, 1995

ABSTRACT **To analyze cotranslational folding of influenza hemagglutinin in the endoplasmic reticulum of live cells, we used short pulses of radiolabeling followed by immunoprecipitation and analysis with a two-dimensional SDS/polyacrylamide gel system which was nonreducing in the first dimension and reducing in the second. It separated nascent glycopolypeptides of different length and oxidation state. Evidence was obtained for cotranslational disulfide formation, generation of conformational epitopes, N-linked glycosylation, and oligosaccharide-dependent binding of calnexin, a membrane-bound chaperone that binds to incompletely folded glycoproteins via partially glucose-trimmed oligosaccharides. When glycosylation or oligosaccharide trimming was inhibited, the folding pathway was perturbed, suggesting a role for N-linked oligosaccharides and calnexin during translation of hemagglutinin.**

Most glycoproteins are synthesized by membrane-bound ribosomes and cotranslationally translocated into the endoplasmic reticulum (ER). Folding and oligomeric assembly occur in the ER lumen prior to transport to the Golgi complex and beyond (1, 2). While translation and translocation are still ongoing, several modifications occur on the luminal side of the ER membrane, including signal-peptide cleavage, N-linked glycosylation, and trimming of glucose residues from the newly added core oligosaccharides. That folding may also begin cotranslationally is known for two proteins, IgG and serum albumin (3, 4), but it is unclear how common and how extensive it is, how it progresses with increasing chain length, and whether it involves chaperones.

To monitor the folding of nascent polypeptides in living tissue culture cells, we took advantage of a two-dimensional SDS/PAGE system to separate full-length and partially synthesized forms of influenza hemagglutinin (HA). This system allowed us to analyze a whole collection of authentic nascent chains. Our results not only provided evidence for cotranslational, chaperone-mediated folding of HA but allowed us to determine when specific disulfide bonds were formed, when N-linked oligosaccharides were added, and what effects various inhibitors had on the cotranslational folding process.

MATERIALS AND METHODS

Virus, Cell Line, Reagents, and Antibodies. The X31 strain of influenza virus A/Aichi/68 and Chinese hamster ovary (CHO) cells were propagated and used as described (5). All reagents were purchased from Sigma with the exception of 3-[(3-cholamidopropyl)dimethylammonio]-1-propanesulfonate (CHAPS), which was from Pierce. A mixture of [^{35}S]methionine and [^{35}S]cysteine was purchased from Amersham. The rabbit polyclonal anti-HA antibody (α-NHA) was raised against the N terminus of HA (residues 1–12). The rabbit polyclonal anti-calnexin antibody (α-CNX) was raised against the C terminus of calnexin (residues 555–573) and affinity purified against the peptide. Mouse monoclonal antibodies against various epitopes of HA of the X31 strain were made from hybridoma cell lines provided by J. Skehel (Medical Research Council, London).

Metabolic Labeling and Immunoprecipitation. CHO cells were infected with X31 influenza virus and metabolically labeled as described (5), except that 200 μCi (1 μCi = 37 kBq) of ^{35}S label was used for each 60-mm culture dish. Cell lysis and immunoprecipitation with α-NHA and mouse monoclonal antibodies against various epitopes of HA were performed as described (6). The two-step sequential precipitation protocol (α-CNX/α-NHA) was performed as described (7) except that CHAPS was used instead of sodium cholate. The antibody for the first immunoprecipitation was α-CNX. After elution in SDS and quenching with Triton X-100, α-NHA was used for the second immunoprecipitation.

Two-Dimensional SDS/PAGE. A minigel apparatus (Hoefer Scientific Instruments) was used according to the manufacturer's instructions. In both dimensions, 7.5% polyacrylamide resolving gels with standard stacking gels were used. Nonreduced immunoprecipitate samples were loaded in the first-dimension tube gel (1.5 mm in diameter). For size determination, alkylated molecular weight standards were sometimes mixed with the immunoprecipitate samples. After electrophoresis in the first dimension, each tube gel was extruded from the gel tube, incubated in 1.5 ml of sample buffer with 0.1 M dithiothreitol (DTT) at 95°C for 10 min, and placed on top of the second-dimension slab gel (1.5 ml in thickness). Fixing, staining, and fluorography were as described (5).

RESULTS

Two-Dimensional SDS/PAGE to Study Nascent Chains. To analyze folding and other events that occur during the translation and translocation of HA, we used a pulse–chase approach combined with immunoprecipitation. The samples were analyzed by a two-dimensional SDS/PAGE method in which the first dimension was without reduction and the second with reduction. Such two-dimensional gels have been used in the past to analyze whether polypeptides are connected by interchain disulfide bonds (8). Since the disulfide-crosslinked polypeptides migrate more slowly in the first dimension than the individual glycopeptides in the second, the spots will be located above the diagonal. In contrast, proteins that do not contain disulfides will be located on the diagonal because they migrate with the same rate before and after reduction (Fig. 1).

In this study, we were specifically interested in polypeptides that would migrate *below* the diagonal because such mobility

The publication costs of this article were defrayed in part by page charge payment. This article must therefore be hereby marked "*advertisement*" in accordance with 18 U.S.C. §1734 solely to indicate this fact.

Abbreviations: ER, endoplasmic reticulum; HA, influenza hemagglutinin; DTT, dithiothreitol; CHAPS, 3-[(3-cholamidopropyl)dimethylammonio]-1-propanesulfonate.

*Present address: University of Amsterdam, Academic Medical Center, Department of Biochemistry, School of Medicine, Meibergdreef 15, 1105 AZ Amsterdam, The Netherlands.

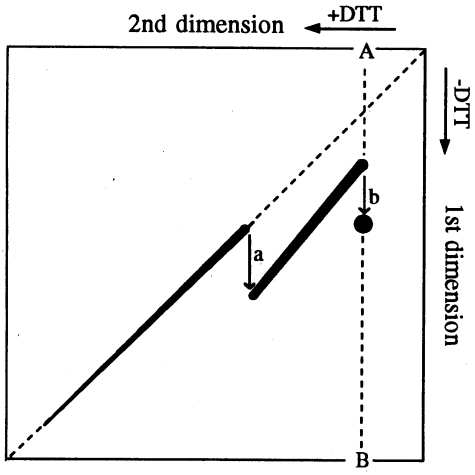

FIG. 1. Effect of co- and posttranslational disulfide bond formation on the mobility of nascent and full-length polypeptide chains in two-dimensional nonreducing/reducing SDS/PAGE. This polypeptide acquires one disulfide bond cotranslationally, arrow *a*, and another one posttranslationally, arrow *b*. It is assumed that the bonds arise synchronously in all the chains. The full-length form of the polypeptide is on the A–B line determined by the molecular weight of the final protein. The nascent chains are located in spurs to the left of the A–B line. The diagonal marks the mobility of reduced proteins.

would be indicative of intrachain disulfide bonds. Proteins that have intrachain disulfides migrate faster in SDS/polyacrylamide gels when nonreduced than when reduced (5). In a two-dimensional nonreducing/reducing gel, a spot below the diagonal would therefore be diagnostic of one or more intrachain disulfide bonds.

Fig. 1 shows schematically the two-dimensional pattern expected for the nascent and full-length chains of a protein with two disulfide bonds, *a* and *b*. The full-length form of the polypeptide is located on the A–B line determined by the final molecular weight. The nascent chains, having lower molecular weights, are localized in spurs to the left of the A–B line. The intensity of labeling within the spurs increases with molecular weight because the longer the chain, the more incorporated label it contains. The shorter nascent chains that do not have disulfides are located on the diagonal, while the longer ones with disulfide *a* in place are found below the diagonal. The location of the abrupt shift from the diagonal reveals the molecular weight at which disulfide *a* is formed. A second shift occurs on the A–B line indicating that disulfide *b* forms posttranslationally. If the sample had been reduced before separation in the first dimension, the full-length and nascent forms would all have run on the diagonal.

Disulfide Formation in Nascent Chains. We applied this system to nascent and full-length influenza HA in infected CHO cells. HA is a type I membrane glycoprotein with seven N-linked oligosaccharides and six intrachain disulfides (Fig. 2*a*) (9). While four of the N-linked glycans are clustered close to the N terminus, the cysteine and methionine residues are relatively evenly distributed throughout the length of the molecule. The oxidized mature ER form (called NT) runs considerably faster than its reduced counterpart R (5). Two partially oxidized full-length folding intermediates, IT1 and IT2, which have intermediate mobilities, have been extensively characterized (5). A cysteine mutagenesis study has shown that IT1 corresponds to a population of intermediates that contain one or more undefined smaller disulfide loops but lack both major loop-forming disulfides, 14–466 and 52–277. IT2 lacks only one of them (14–466) (Fig. 2*a*) (I.B., B. Foellmer, and A.H., unpublished data). The observation that cells do not contain reduced full-length HA chains (R) has previously led to the conclusion that one or more disulfide bonds form already on the nascent chains (5), but it is unclear how extensive nascent-chain folding might be.

To label the nascent chains, the infected cells were given a short pulse of [^{35}S]methionine and [^{35}S]cysteine. They were then treated with *N*-ethylmaleimide to prevent further oxidization (5), and the nascent and full-length HA polypeptides were isolated by immunoprecipitation with α-NHA. Since the pulse (1.5 min) was shorter than the 2.0-min average synthesis time of HA (5), the majority of the label was expected to be in nascent chains.

After one-dimensional SDS/PAGE of reduced samples and fluorography, the nascent chains were seen as a broad, uneven smear below the band of full-length HA (Fig. 2*b*, lane 1). When the samples were electrophoresed without prior reduction, the full-length HA migrated as three faster migrating bands corresponding to the two partially oxidized folding intermediates, IT1 and IT2, and the fully oxidized HA called NT (Fig. 2*b*, lane 2), but the IT2 and NT bands were all but covered by the smear of nascent chains.

After two-dimensional electrophoresis, the full-length and nascent chains were separated. The full-length HA (IT1, IT2, and NT) formed three spots below the diagonal. The spur-like traces that emanated from these spots contained the nascent chains (Fig. 2*c*). The spurs associated with the IT1 and IT2 spots were composed of nascent chains because they were transient—i.e., they disappeared after a short chase (Fig. 2*e*). When folding was performed posttranslationally by a DTT washout protocol (6), no spurs were observed (data not shown).

Unlike the spurs coming from IT1 and IT2, the short spur associated with the NT spot was present in the controls, indicating that at least some of the HA in this short tail corresponded to a population of full-length HA molecules. Perhaps it contained HA that had undergone extensive trimming of the N-linked oligosaccharides. When the samples were run reduced in both directions, or when the pulse was done in the presence of 5 mM DTT to prevent disulfide formation (Fig. 2*d*), both nascent and full-length HA chains were seen on the diagonal.

The length of the spurs, their position, their relative intensity, and the distribution of radioactivity within them provided information about a variety of cotranslational events. The spur emanating from IT1 followed the diagonal for most of its length, but a slight bend in the upper part as it joined the IT1 spot implied that some of the smaller disulfides may have begun to form cotranslationally. The spur radiating from the IT2 spot in Fig. 2*c* indicated more clearly that disulfide 52–277 could form already on the nascent chains. Unlike disulfide *a* in the hypothetical example in Fig. 1, the formation of this disulfide was clearly not synchronous in all the chains. When the radioactivity was measured by a phosphor imager, it was found that one out of five HA chains formed this bond before chain termination. The length of the spur indicated that formation of the disulfide could begin at the earliest when the chains had reached a size of 63 kDa. Given the known average elongation rate of HA (four to five residues per second, ref. 5), we estimated that oxidation of the bond commenced about 30 sec after the second cysteine of the pair (cysteine-277) had entered the ER lumen.

When the nascent chains were given more time to fold—by arresting synthesis with an elongation inhibitor, cycloheximide—the disulfide bonds were found to form at earlier stages of translation, and they formed more efficiently (Fig. 2*f*). Under these conditions, the start of the IT2 spur was closer to a gap which corresponded to the addition of a glycan to asparagine-285 (see below).

Cotranslational Glycosylation. The distribution of radioactivity within the spurs was uneven. The region of high radioactivity marked with an arrowhead in Fig. 2*c* most likely corresponded to ribosome stacking at an elongation pause site

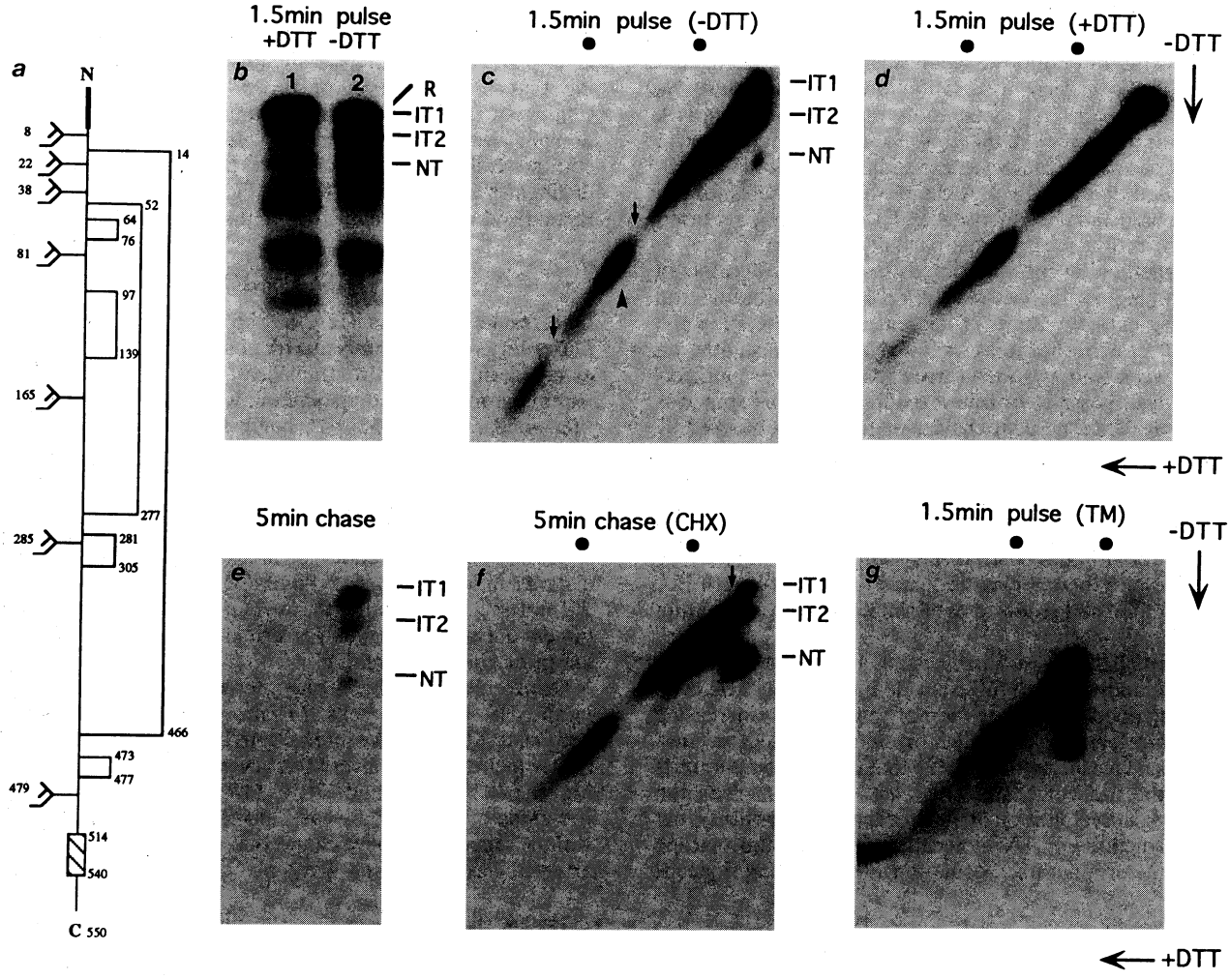

FIG. 2. Cotranslational folding of HA analyzed by one- and two-dimensional SDS/PAGE. CHO cells infected with influenza virus A/Aichi/68 (X31) were radiolabeled 5 hr postinfection for 1.5 min. Either immediately after the pulse or after a 5-min chase, the cells were flooded with phosphate-buffered saline containing 20 mM *N*-ethylmaleimide to alkylate free sulfhydryls. After detergent solubilization in the continued presence of *N*-ethylmaleimide, the postnuclear supernatant was immunoprecipitated with antibodies against the N-terminal peptide (residues 1–12) of HA (α-NHA) and analyzed by one- or two-dimensional SDS/PAGE. (*a*) Schematic drawing of HA's structure. The positions of disulfide bonds and N-linked glycans are shown. The N-terminal signal sequence and the C-terminal transmembrane region are represented by a thick bar and a hatched box, respectively. (*b*) One-dimensional SDS/PAGE analysis of the 1.5-min-pulsed immunoprecipitates either with (lane 1) or without (lane 2) prior reduction. (*c*) Two-dimensional SDS/PAGE analysis of the 1.5-min-pulsed sample. (*d*) Sample from cells pulsed for 1.5 min in the presence of 5 mM DTT. (*e*) Sample from cells pulsed for 1.5 min and chased for 5 min. (*f*) Sample from cells pulsed for 1.5 min and chased for 5 min in the presence of 1 mM cycloheximide (CHX). (*g*) Sample from cells preincubated for 45 min and pulsed for 1.5 min in the presence of tunicamycin (TM, 5 μg/ml). The accumulation of radioactivity at the bottom left in this gel was due to the dye front. The two closed circles above the two-dimensional gels denote the mobility of two molecular size markers, bovine serum albumin (66 kDa) and chicken egg-white albumin (45 kDa).

(10). The gaps reproducibly observed at nascent chain sizes of 35 and 50 kDa (marked in the IT1 spur with arrows) were absent when translation was performed in the presence of tunicamycin, an inhibitor of N-linked glycosylation (Fig. 2*g*). They were therefore most likely caused by core glycan addition to asparagine residues 165 and 285. Their position and sharpness indicated that, unlike disulfide formation, core oligosaccharide addition occurred synchronously in all the chains and that the glycans were transferred almost immediately to the polypeptide when the consensus acceptor site for glycosylation entered the lumen of the ER.

A third gap, corresponding to the most C-terminal one of the glycosylation sites (asparagine-479), is best appreciated in Fig. 2*f* (marked with an arrow) because it is normally obscured by the strong IT1 and IT2 spots. Since this last glycan is only 71 residues from the C terminus, the timing of its addition must be close to or after chain completion (the ribosome contains about 40 residues and the transmembrane segment at least 10; ref. 11).

By preventing the addition of N-linked oligosaccharides, tunicamycin is known to prevent proper folding of HA and eventually cause the formation of aggregates crosslinked by aberrant interchain disulfides (12). The two-dimensional gel analysis in Fig. 2*g* showed, as expected, that the full-length unglycosylated HA had a lower molecular weight. Interestingly, deviation from normal folding was already apparent during translation.

Association with Calnexin. N-linked glycans undergo glucose trimming immediately after addition to the growing polypeptide chain (13, 14). Removal of two glucose residues allows HA to associate with calnexin, a lectin-like chaperone in the ER membrane (15). Calnexin binds transiently to many glycoproteins during their folding and oligomeric assembly in the ER and is needed for their retention in the ER and their proper folding (16, 17). Since calnexin binds to IT1 and IT2 (15), it was of interest to determine whether the association began on the nascent chain. A sequential precipitation protocol (7) with α-CNX and α-NHA was used.

About 20% of the nascent HA chains coprecipitated with calnexin (Fig. 3*a*). The length of the spur indicated that association started before the chain was half-completed, suggesting that the earliest association involved the more N-terminal four glycans. No association was detected when HA synthesis was performed in the presence of either tunicamycin (Fig. 3*c*) or castanospermine, a glucosidase inhibitor (Fig. 3*d*). We concluded that nascent HA chains were substrates for the membrane-associated chaperone and that binding required that glucose residues be at least partially trimmed.

To test whether the cotranslational association with calnexin or the trimming of glucoses played a role in HA folding, the two-dimensional gel pattern of nascent chains labeled in the presence of castanospermine was analyzed. Consistently, an additional weak spur was seen (arrowhead in Fig. 3*b*) indicating premature, possibly transient oxidization. This spur was more obvious when nascent chain elongation was blocked by cycloheximide (arrowhead in Fig. 3*e*). Moreover, a weak but reproducible high molecular weight smear above the diagonal at the molecular weight of full-length HA (marked as AGG for "aggregate" in Fig. 3*e*) indicated that crosslinked oligomeric complexes were formed posttranslationally as a misfolded side product. Despite these anomalies, most of the full-length HA reached a folded and oxidized conformation (NT) after 5 min of chase.

Formation of Epitopes. Finally, using a panel of conformation-specific antibodies to different domains of the HA molecule, we mapped the progression of folding with increasing nascent chain length. Antibodies to epitope A, located in a prominent surface loop (9), revealed that the top domain starts to fold in the nascent chains (Fig. 4*a*). However, given the relatively weak precipitation of nascent chains, it was likely that only a subfraction of HA molecules expressed the epitope before chain termination. Formation of another epitope, E (Fig. 4*b*), located somewhat further down in the top domain, and a stem-domain epitope, F2 (Fig. 4*d*), occurred later. Epitopes E and F2 were specific for the IT2 spur, demonstrating that the formation of the 52–277 disulfide played a significant role in the cotranslational folding of both the top domain and the stem domain. Antibodies to a stem-domain epitope called F1 (Fig. 4*c*), on the other hand, did not distinguish between the IT1 and IT2 spurs. It, however, only recognized nascent chains larger than 68 kDa.

DISCUSSION

Our results show that HA folding starts cotranslationally. Different parts of a nascent HA chain can be simultaneously engaged in translation, translocation, glycosylation, glycan trimming, folding, and association with calnexin. Some disulfide bonds, notably 52–277, begin to form soon after both cysteines in the pair have entered the ER lumen. However, since only one out of five chains acquires this bond before chain termination, it is clear that cotranslational folding is nonsynchronous within the population of nascent chains. At least some nascent chains undergo calnexin binding, and this association can begin when the chains are about half translated. We did not see evidence for the formation of aberrant disulfide bonds, unless folding was perturbed by inhibitors to glycosylation or glucose trimming.

Our results show chaperone interaction with nascent chains in the ER of living cells. *In vitro* translation studies have demonstrated extensive interactions between nascent chains of firefly luciferase and a variety of cytosolic chaperones, including Hsp40, Hsp70, and TRiC (18), and between arrested pro-α-factor and BiP in yeast microsomes (19). These observations suggest extensive chaperone interactions, at least with arrested nascent chains. Evidence of *in vivo* interaction be-

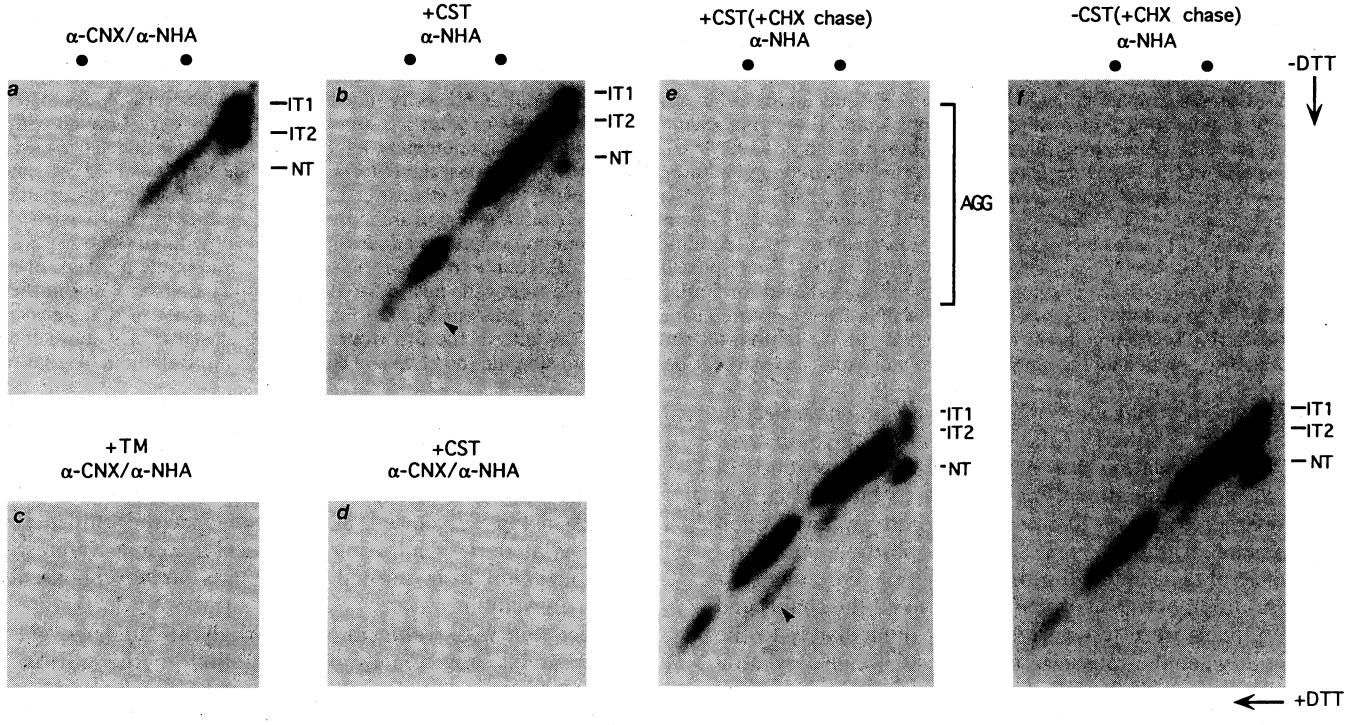

FIG. 3. Cotranslational association of HA with calnexin. (*a*) Infected CHO cells were pulsed for 1.5 min, and the lysate was immunoprecipitated sequentially with anti-calnexin (α-CNX) and antibody to the N terminus (residues 1–12) of HA (α-NHA). (*b*) Sample from cells pretreated for 30 min with 1 mM castanospermine (CST), pulse labeled for 1.5 min in the presence of CST, and immunoprecipitated with α-NHA. (*c*) Sample from cells pretreated with tunicamycin (TM, 5 μg/ml) for 45 min, pulse-labeled for 1.5 min in the presence of TM, and immunoprecipitated sequentially with α-CNX and α-NHA. (*d*) Same sample as in *b* immunoprecipitated sequentially with α-CNX and α-NHA. (*e*) Sample from cells pretreated with 1 mM CST, pulse labeled for 1 min in the presence of CST, chased for 5 min with 1 mM cycloheximide (CHX) in the continued presence of 1 mM CST, and immunoprecipitated with α-NHA. The shorter pulse resulted in a higher percentage of label in the nascent chains. (*f*) Same as in *e*, except no CST was present at any stage. Molecular size markers are the same as in Fig. 2.

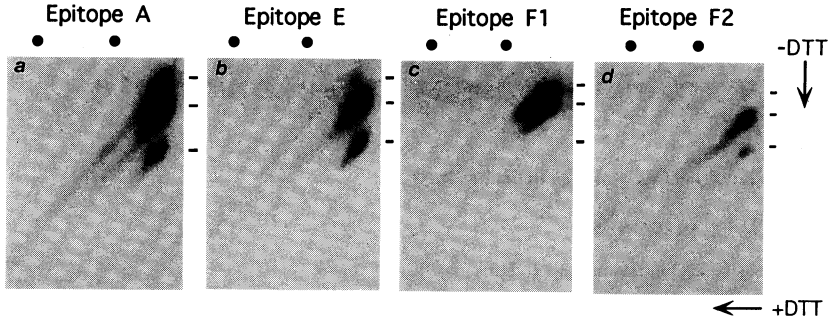

FIG. 4. Cotranslational epitope formation in HA. Lysate from influenza-infected CHO cells pulsed for 1.5 min (as in Fig. 2*c*) was immunoprecipitated with mouse monoclonal antibodies (mAbs) against various epitopes. The immunoprecipitates were analyzed by two-dimensional SDS/PAGE. (*a*) mAb HC113 against top-domain epitope A. (*b*) mAb HC45 against top-domain epitope E. (*c*) mAb F1 against stem-domain epitope F1. (*d*) mAb F2 against stem-domain epitope F2. Positions of IT1, IT2, and NT are marked by short bars to the right of each gel. Molecular size markers are as in Fig. 2.

tween nascent chain and cytosolic Hsp70 was obtained through coprecipitation of polysome-bound nascent chains by cytosolic Hsp70 antibody (20). Our attempts to detect BiP binding to nascent chains of HA have been unsuccessful in live cells. Preliminary results indicate, however, that BiP does associate with nascent vesicular stomatitis virus glycoproteins in infected cells (W.C. and A.H., unpublished results).

The translocation complex in the ER membrane constitutes a large transmembrane assembly that contains the ribosome, ribosome receptor, channel components, signal peptidase subunits, and a multimeric oligosaccharide transferase (21). According to our results, it must also accommodate glucosidases I and II, as well as the membrane-bound molecular chaperone, calnexin, which assists the folding of the translocating glycopolypeptide chains.

While not always necessary for proper folding (6, 22), the cotranslational folding process can help to prevent nonproductive side reactions. It may allow folding to progress in an orderly domain-by-domain sequence. This may be particularly crucial for the folding of large polypeptide chains with many linearly arranged domains. Many such proteins are synthesized in the ER. The gel system introduced here for analyzing nascent chains may provide a generally applicable technique for learning more about the elusive and neglected events that occur coincidentally with translation.

We thank Dr. J. Skehel for hybridoma cell lines, M. Ittensohn for help with the monoclonal antibodies, and H. Tan for photographic work. We are thankful to J. Weissman, J. F. Simons, and other members of the Helenius–Mellman group for advice. Funding was obtained from the National Institutes of Health (GM38346 and CA46128) and the Human Frontiers Science Program.

1. Hurtley, S. M. & Helenius, A. (1989) *Annu. Rev. Cell Biol.* **5,** 277–307.
2. Klausner, R. D. (1989) *New Biol.* **1,** 3–8.
3. Bergman, L. W. & Kuehl, W. M. (1979) *J. Biol. Chem.* **254,** 8869–8876.
4. Peters, T., Jr., & Davidson, L. K. (1982) *J. Biol. Chem.* **257,** 8847–8853.
5. Braakman, I., Hoover-Litty, H., Wagner, K. R. & Helenius, A. (1991) *J. Cell Biol.* **114,** 401–411.
6. Braakman, I., Helenius, J. & Helenius, A. (1992) *EMBO J.* **11,** 1717–1722.
7. Ou, W.-J., Cameron, P. H., Thomas, D. Y. & Bergeron, J. J. M. (1993) *Nature (London)* **364,** 771–776.
8. Sommer, A. & Traut, R. R. (1974) *Proc. Natl. Acad. Sci. USA* **71,** 3946–3950.
9. Wiley, D. C. & Skehel, J. J. (1987) *Annu. Rev. Biochem.* **56,** 365–395.
10. Protzel, A. & Morris, A. J. (1974) *J. Biol. Chem.* **249,** 4594–4600.
11. Smith, W. P., Tai, P. C. & Davis, B. D. (1978) *Proc. Natl. Acad. Sci. USA* **75,** 5922–5925.
12. Hurtley, S. M., Bole, D. G., Hoover-Litty, H., Helenius, A. & Copeland, C. S. (1989) *J. Cell Biol.* **108,** 2117–2126.
13. Kornfeld, R. & Kornfeld, S. (1985) *Annu. Rev. Biochem.* **54,** 631–664.
14. Atkinson, P. H. & Lee, J. T. (1984) *J. Cell Biol.* **98,** 2245–2249.
15. Hammond, C., Braakman, I. & Helenius, A. (1994) *Proc. Natl. Acad. Sci. USA* **91,** 913–917.
16. Bergeron, J. J. M., Brenner, M. B., Thomas, D. Y. & Williams, D. B. (1994) *Trends Biochem. Sci.* **19,** 124–128.
17. Hammond, C. & Helenius, A. (1994) *Science* **266,** 456–458.
18. Frydman, J., Nimmesgern, E., Ohtsuka, K. & Hartl, F. U. (1994) *Nature (London)* **370,** 111–117.
19. Sanders, S. L., Whitfield, K. M., Vogel, J. P., Rose, M. D. & Schekman, R. W. (1992) *Cell* **69,** 353–365.
20. Beckmann, R. P., Mizzen, L. A. & Welch, W. J. (1990) *Science* **248,** 850–853.
21. Gilmore, R. (1993) *Cell* **75,** 589–592.
22. Tatu, U., Braakman, I. & Helenius, A. (1993) *EMBO J.* **12,** 2151–2157.